Journal of Materials Chemistry A

PAPER

View Article Online
View Journal | View Issue

Cite this: J. Mater. Chem. A, 2017, 5, 1472

The direct hydrothermal deposition of cobalt-doped MoS_2 onto fluorine-doped SnO_2 substrates for catalysis of the electrochemical hydrogen evolution reaction†

Isolda Roger,‡[a] Roberta Moca,‡[a] Haralampos. N. Miras,[a] Kevin G. Crawford,[b] David A. J. Moran,[b] Alexey Y. Ganin*[a] and Mark D. Symes*[a]

Received 23rd September 2016
Accepted 10th December 2016

DOI: 10.1039/c6ta08287d

www.rsc.org/MaterialsA

Metal chalcogenides, and doped molybdenum sulfides in particular, have considerable potential as earth-abundant electrocatalysts for the hydrogen evolution reaction. This is especially true in the case of solar-to-hydrogen devices, where an ability to deposit these materials on transparent substrates is therefore desirable. Hydrothermal methods are perhaps the most common route by which metal chalcogenide materials suitable for the hydrogen evolution reaction are produced. Such methods are simple and scalable, but the direct hydrothermal deposition of metal chalcogenides on transparent oxide electrodes has hitherto never been reported. Such an advance would greatly facilitate the expansion of the field by removing the requirement for separate hydrothermal-synthesis and catalyst-deposition steps. In this paper, we show that the ternary chalcogenide $Co_2Mo_9S_{26}$ can be synthesised on a fluorine-doped tin oxide substrate by hydrothermal methods directly from solutions of the simple metal salts. These films display good activity for the hydrogen evolution reaction from acid solution, achieving current densities of 10 mA cm^{-2} at 260 mV overpotential with a Tafel slope of 64 mV per decade. Moreover, the resulting films can be made to be translucent, a very useful property which would allow light to be transmitted through the catalyst to an underlying light-harvesting array in any solar-to-hydrogen device employing this material at the cathode.

Introduction

Metal chalcogenides are a fascinating class of materials with properties conducive to catalysis,[1–3] energy storage,[4–7] photovoltaics,[8,9] electronic devices[10–12] and sensing applications.[13,14] Amongst the more promising potential applications of metal-chalcogenides, their use as cathodes for electrochemical water splitting has attracted significant attention in recent years.[15] Much of this interest stems from the prospect of replacing platinum as the cathode in solar-driven water splitting devices with materials that are both cheaper and more abundant. In this regard, molybdenum sulfides of various compositions (Mo_xS_y) have been shown to be highly effective hydrogen evolution catalysts from aqueous solution over a wide pH-range.[16,17] Moreover, doping of molybdenum sulfides with other transition metals has been proposed as a route to improving electrocatalytic activity for hydrogen evolution.[18,19] This is especially true in the case of cobalt, with various $CoMoS_x$-type materials having been prepared and shown to outperform undoped MoS_2.[20–24]

With regard to the synthesis of metal chalcogenides, hydrothermal routes are particularly desirable due to their relative simplicity and scalability. Mo_xS_y species have been synthesised on glassy carbon and other non-transparent supports by hydrothermal methods on several occasions (see, for example, ref. 25–30), but the direct hydrothermal synthesis of MoS_2 on transparent oxide electrodes has yet to be reported. Such an advance would be of great utility in integrating Mo_xS_y-based materials into solar-to-fuels devices, as it would allow this promising class of hydrogen evolution catalysts to be deposited directly onto the electrode substrate hydrothermally without the need for further processing steps. However, the harsh environment that characterises aqueous solutions under typical hydrothermal conditions tends to strip the transparent conductive metal-oxide layer from the electrode support (often glass), and hence the direct hydrothermal formation of Mo_xS_y species on transparent electrodes has hitherto been overlooked or assumed to be impractical.

Herein, however, we show that the hydrothermal synthesis of metal-chalcogenides directly onto transparent metal-oxide

[a]WestCHEM, School of Chemistry, University of Glasgow, University Avenue, Glasgow, G12 8QQ, UK. E-mail: mark.symes@glasgow.ac.uk; alexey.ganin@glasgow.ac.uk
[b]School of Engineering, University of Glasgow, Glasgow G12 8LT, UK

† Electronic supplementary information (ESI) available: XPS, and additional electrochemical and SEM data. See DOI: 10.1039/c6ta08287d

‡ These authors contributed equally to this work.

electrodes is indeed possible, and that the resulting decorated electrodes remain conductive and have metrics for the hydrogen evolution reaction from 0.5 M H_2SO_4 that are comparable to those obtained from similar materials on transparent metal-oxide electrodes but that were prepared by other (non-hydrothermal) methods. In particular, we demonstrate the potential of this approach by synthesising a ternary chalcogenide with composition $Co_2Mo_9S_{26}$ directly on fluorine-doped tin oxide (FTO) electrodes, which we then show to display good activity for the hydrogen evolution reaction in aqueous solution, achieving current densities of 10 mA cm^{-2} at 260 mV overpotential.

Results and discussion

Synthesis and characterisation of Co-doped molybdenum sulfide on fluorine-doped tin oxide (FTO)

Samples of Co-doped molybdenum sulfide were prepared directly on FTO substrates by hydrothermal methods (see Experimental section for a detailed description). Briefly, aqueous solutions containing the simple metal salts (cobalt sulfate and ammonium heptamolybdate) were mixed with thiourea in the appropriate ratios before being transferred to 20 mL Teflon-lined bombs. Into each bomb was placed a single 1 × 2.5 cm^2 FTO-on-glass slide (with the FTO coating on one side of the slide only) at a 45° angle to both the base and side of the reaction chamber (see ESI, Fig. S1†). The bombs were then sealed and heated at a rate of 1 °C min^{-1} up to a temperature of 180 °C. Films heated to 230 °C adhered very poorly to the FTO substrate, and delaminated rapidly upon subsequent immersion in electrolyte solutions. Hence a temperature of 180 °C was used for producing all the films reported in this manuscript. This temperature was then maintained for 72 hours before cooling at a rate of 10 °C min^{-1} back to room temperature. After extrication of the FTO slides from the bombs and washing with water to remove loosely-held material, robust, grey-black films were evident on the conductive (FTO) side of the substrates only. This was true whether the FTO side of the substrate faced upwards or downwards in the bomb, and indeed the properties of the films (described below) showed no dependence on whether the FTO side of the substrate faced upwards or downwards.

Removal of the deposited film from the FTO side of the substrate by mechanical scratching revealed that the underlying FTO layer was still conductive. In contrast, FTO-on-glass slides that were heated hydrothermally in the same manner but in the absence of any metal salts suffered degradation of their FTO layer and became non-conductive. When samples were prepared using a solution containing only ammonium heptamolybdate and thiourea (*i.e.* without the addition of cobalt salts to the deposition solution), black films were again produced on the conductive side of the FTO substrates, but these films delaminated from the substrate almost instantly upon immersion in electrolyte solutions (in contrast to films formed from solutions containing both molybdenum and cobalt precursors). Moreover, no film formation was observed from precursor solutions that contained only cobalt sulfate and thiourea (*i.e.* in the absence of molybdenum). Hence it was concluded that the formation of metal-chalcogenide films on these FTO substrates was possible without the degradation of the fluorine-doped SnO_2 layer under hydrothermal conditions, and that the presence of both cobalt and molybdenum in the precursor solutions was required in order to produce films stable enough for subsequent electrochemical analysis (see below). However, it is not apparent whether the FTO substrate is actively protected by the deposited films, or whether the reaction medium from which these films are deposited is inherently less corrosive towards FTO than reaction media that lack these metal ions.

Films formed on FTO hydrothermally from solutions containing 2.3 mM Co(II), 13.6 mM Mo(VI) and 34.1 mM thiourea were examined by Atomic Force Microscopy (AFM) and found to have an average thickness on the order of 300 nm (±50 nm) – see Experimental methods and Fig. S2.† Analysis of these films by atomic adsorption spectroscopy evinced an average relative weight percentage of Mo 47.4 wt% and Co 6.5 wt%. This translates to a Co : Mo ratio of 1 : 4.5 (somewhat below the ratio of 1 : 6 in the deposition solution). CHN analysis of the films indicated that the levels of carbon, hydrogen and nitrogen present were all negligible. Therefore, assuming that the residual mass in the atomic adsorption data is due to sulfur, we assign a formula of $CoMo_{4.5}S_{13}$ ($Co_2Mo_9S_{26}$) to this hydrothermally-produced material. Assuming a crystallographic density of $Co_2Mo_9S_{26}$ of 4.87 g cm^{-3} (estimated using the Diamond 3.0 program[31]), the typical mass loading of this material on the FTO substrates thus equates to ~0.15 mg cm^{-2}.

According to X-ray diffraction (XRD) (Fig. 1), these films are polycrystalline in nature and show a broad (002) reflection peak corresponding to the layered hexagonal structure of MoS_2. The PXRD pattern of a blank FTO slide is given for comparison (Fig. 1b), showing that the majority of the reflections arise from the underlying FTO substrate. This is in line with our observation that the deposition of the metal chalcogenide film is possible without the degradation of the substrate FTO layer. Due to the lack of significant reflections, the only parameter that could be estimated for the metal chalcogenide films was

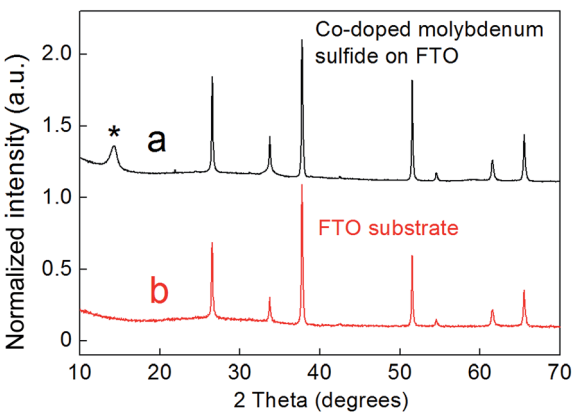

Fig. 1 (a) XRD pattern of a Co-doped molybdenum sulfide film grown on an FTO substrate (black). The peak associated with the hexagonal structure of MoS_2 is highlighted with the asterisk. (b) The XRD pattern of a blank FTO substrate for comparison (red).

$c = 12.36$ Å, which nevertheless is in good agreement with the value expected for an MoS_2 phase. No reflections from adversary crystalline phases were observed within the pattern, suggesting that both Co and Mo are incorporated within the same structure.

Two dominant peaks were observed by Raman spectroscopy of the bulk sample at 374 and 403 cm^{-1}, corresponding to the in-plane (E^1_{2g}) vibration and the out-of-plane A_{1g} mode respectively – values which are typical for MoS_2 (Fig. 2).[32,33] The peak separation ($\Delta k = 29$ cm^{-1}) agrees with values reported for bulk MoS_2.[34] Furthermore, no peaks associated with the presence of either CoS_x or MoO_x were observed in the Raman spectrum.

XPS spectroscopy of the films revealed that Mo, Co and S were all present on the surface of the deposited materials. The valence state of molybdenum could be ascertained by examination of the 3d region of the XPS spectrum (Fig. S3†), which revealed two dominant peaks associated with Mo^{IV} ions (corresponding to about 87 atomic% of the total molybdenum). Other minor components were also observed, and were attributed to Mo^{V} and Mo^{VI} ions, probably associated with the presence of 6.5 atomic% MoO_2OH and 6.5 atomic% MoO_3 on the surface of the sample, in agreement with reported XPS spectra of MoS_2 (see, for example, ref. 35 and 36). The presence of cobalt on the surface of the films was confirmed by a high resolution spectrum in Co 2p region, which showed two doublets (suggesting a mixed valence state of 57 atomic% Co^{2+} and 43 atomic% Co^{3+}, Fig. S4†). Again, it is possible that there is some contribution from Co-oxides to this signal. The peaks in the S $2p_{3/2}$ region of the spectrum could be fitted with a single doublet (with binding energies 162.2 and 163.4 eV), which agrees with an assignment of the sulfur's oxidation state on the surface as being S^{2-} (Fig. S5†).

The morphology of the products as assessed by scanning electron microscopy (SEM) showed the films to be homogeneous (Fig. S6†). The higher-magnification images indicate that the product films consist of a large number of discrete "sea-urchin-type" blocks probably consisting of randomly-aligned chalcogenide platelets. The presence of such morphology is in agreement with significant peak broadening observed in the PXRD pattern (Fig. 1), which is due to the misalignment of layers along the *c*-axis of the hexagonal structure. Such misfit between the layers is important for the electrochemical properties of these materials, as it generally leads to an increased number of catalytic sites (predominately located at the interfaces and edges of the MoS_2 sheets).[15]

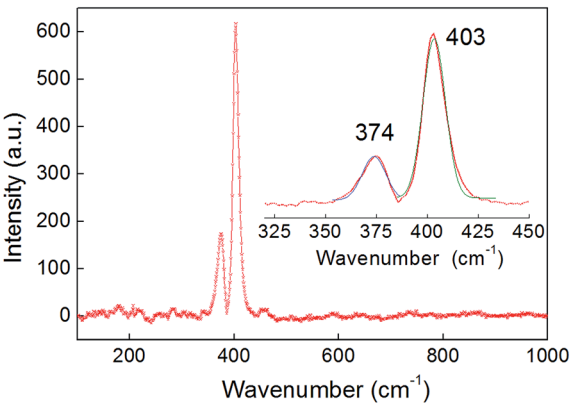

Fig. 2 A wide range Raman spectrum of a 300 nm-thick film deposited on an FTO substrate, which only shows peaks associated with the $Co_2Mo_9S_{26}$ phase. The sample penetration depth was over 100 nm. Inset: a magnified region showing the two peaks associated with the Raman-active in-plane ($E^1_{2g} = 374$ cm^{-1}) and out-of-the-plane ($A_{1g} = 403$ cm^{-1}) modes fitted with Gaussian functions. The peak separation ($\Delta k = 29$ cm^{-1}) is consistent with the bulk character of the film.

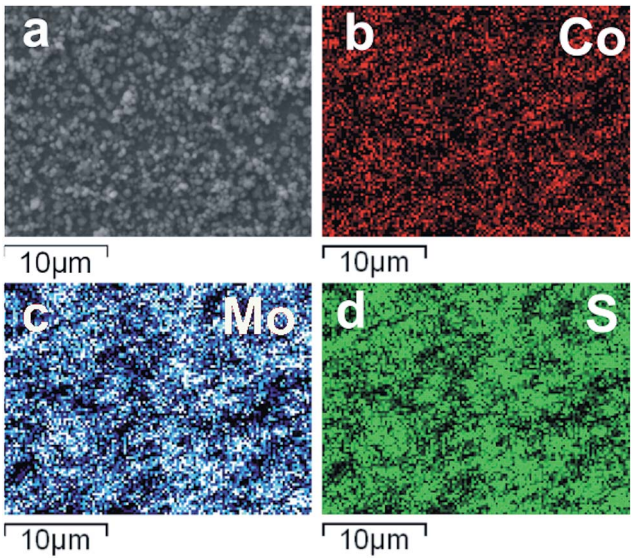

Fig. 3 SEM images and the corresponding elemental mapping for Co, Mo and S in a $Co_2Mo_9S_{26}$ film, indicating the homogeneous distribution of Co atoms within the sample.

Elemental mapping by EDX analysis showed a homogeneous distribution of Co, Mo and S on the surface of the films (Fig. 3), in turn suggesting that Co-atoms replace some of the Mo-atoms within the hexagonal structure of MoS_2. These results agree with those obtained by PXRD where no significant reflections associated with Co–S or Co–O phases were present. Elemental analysis using EDX spectroscopy showed an average Co : Mo ratio of 1 : 5. Whilst it should be noted that EDX can only be used on an indicative, semi-quantitative basis in this case due to the overlapping of the Mo and S peaks in the spectra (see Fig. S6†), this data provides further evidence for the nature of the hydrothermally-deposited material being a ternary chalcogenide with a stoichiometry close to $Co_2Mo_9S_{26}$.

Modification of the standard synthetic procedure by using lower concentrations of cobalt, molybdenum and thiourea in the deposition solutions led to the formation of somewhat thinner films, through which the transmission of light was more evident as shown in Fig. 4. Indeed, employing the same general hydrothermal method described above, but with concentrations of cobalt, molybdenum and sulfur in the deposition solution that were all lower by a factor of 2.5 compared to the standard procedure (see Experimental section), films on the order of 150 nm (±50 nm) thick could be produced (see Fig. S7†). However, further dilution of the precursor solution failed to produce films that covered the FTO substrate in a uniform manner.

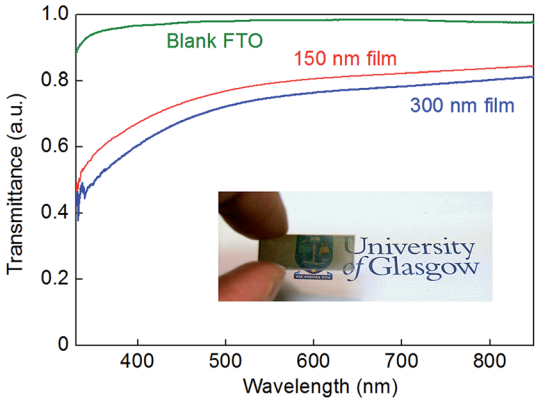

Fig. 4 UV-vis transmission spectra of a 300 nm-thick Co-doped molybdenum sulfide film on FTO (blue line), a 150 nm-thick Co-doped molybdenum sulfide film on FTO (red line), and a blank FTO substrate for comparison (green line). A 1 mm-thick solid metal plate had a transmittance of zero on this scale (data not shown). Inset: a photograph of a 150 nm-thick Co-doped molybdenum sulfide film on FTO showing its translucent nature.

Fig. 4 compares the transmission of light through a 150 nm-thick film alongside the transmission of light through a 300 nm-thick film on FTO and a bare FTO substrate. Thin, translucent, Co-doped molybdenum sulfide films such as those shown in Fig. 4 are of considerable interest given that ternary metal chalcogenides have been proposed as cathode catalysts in solar-to-hydrogen devices (where transmission of light through the electrocatalyst to the underlying light-harvesting material would be desirable). We next, therefore, assessed the competence of our hydrothermally-produced Co-doped molybdenum sulfide films as hydrogen evolution electrocatalysts in aqueous solution.

Hydrothermally-produced Co-doped molybdenum sulfide on FTO as a cathode for the electrochemical hydrogen evolution reaction

The performance of these hydrothermally-produced, Co-doped molybdenum sulfide-on-FTO slides as cathodes for the electrochemical hydrogen evolution reaction was probed in 0.5 M H_2SO_4. Fig. 5a shows how the current density varied with applied potential for these electrodes, as compared to a blank FTO slide (Fig. S8† shows a comparison of the performance of a Co-doped molybdenum sulfide-on-FTO slide as compared to a blank FTO slide under the same conditions by cyclic voltammetry). Hence 300 nm-thick $Co_2Mo_9S_{26}$-on-FTO cathodes were found to deliver a current density of 10 mA cm^{-2} at ~260 mV overpotential (262 mV ± 8 mV). Meanwhile, Tafel analysis of these electrodes in 0.5 M H_2SO_4 gave a slope of 64 ± 2 mV per decade as shown in Fig. 5b. These data were collected by linear sweep voltammetry at slow scan rates (2 mV s^{-1}). A Tafel plot obtained from steady-state current density readings collected by controlled potential electrolysis at various potentials within the range shown in Fig. 5b gave a value in close agreement with that obtained by linear sweep voltammetry (66 mV per decade, see Fig. S9†). Thinner (150 nm-thick films) evinced marginally poorer performance, requiring 300 mV overpotential to deliver a current density of 10 mA cm^{-2}, with a Tafel slope in the region of 85 mV per decade (see Fig. S10 and S11†).

The performance of these films was also tested in 0.5 M sodium phosphate buffer (pH 7) and 1 M NaOH (pH 14). At pH 7, the films exhibited distinctly poorer performance compared to pH 0, achieving a current density of 1 mA cm^{-2} at ~210 mV overpotential, or 10 mA cm^{-2} at ~460 mV overpotential (see Fig. S12†). These films thus show similar performance at pH 7 to the electrodeposited Co-doped MoS_3 films reported by Hu and co-workers[20] on glassy carbon substrates (although we note that these authors do not report current densities higher than 1 mA cm^{-2} for their materials at this pH). Meanwhile, the Tafel slope for our cathodes within the current density range −0.5 to −5 mA cm^{-2} was on the order 220 mV (see Fig. S13†). At pH 14 on the other hand, our $Co_2Mo_9S_{26}$-on-FTO cathodes exhibited very poor stability and the catalyst material was observed to exfoliate into solution rather rapidly during electrochemical analysis, precluding the collection of meaningful hydrogen evolution data.

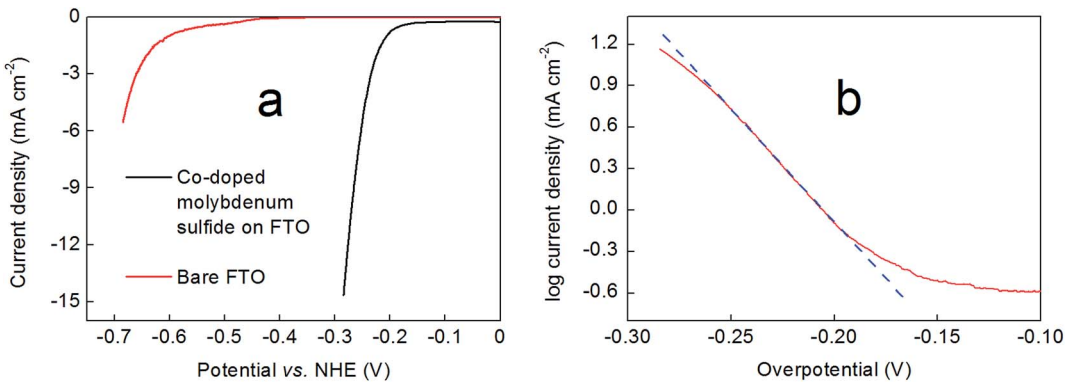

Fig. 5 (a) Comparison of the current densities at pH 0 delivered by a 300 nm-thick $Co_2Mo_9S_{26}$ film prepared by the methods described above on an FTO support (black line) and a bare FTO electrode (red line) obtained by linear sweep voltammetry at a scan rate of 2 mV s^{-1}. (b) A representative Tafel plot collected for a $Co_2Mo_9S_{26}$ film in 0.5 M H_2SO_4 by linear sweep voltammetry (see Experimental section for details). The blue dashed line is provided as a guide to the eye. In both panels, an Ag/AgCl reference electrode and carbon cloth counter electrode were used at room temperature. All current densities have been corrected for resistance.

Table 1 Tafel slopes and overpotentials required to reach a benchmark current density of 10 mA cm^{-2} for a selection of recently-reported metal-chalcogenide HER catalysts on FTO substrates

Entry	Reference	Catalytic material	pH	η at 10 mA cm^{-2} (mV)	Tafel slope[a]	Catalyst deposition method
1	Tran *et al.* (2013) (ref. 23)	$CoMoS_x$	7	250	85	Electrodeposition
2	Tran *et al.* (2012) (ref. 38)	Cu_2MoS_4	0	300	95	Precipitation of simple salts
3	Sun *et al.* (ref. 39)	Cobalt sulfides	7	150	93	Electrodeposition
4	Laursen *et al.* (ref. 40)	MoS_2 on activated carbon	0	210 (5 mA cm^{-2})	—	Electrodeposition
5	Meng *et al.* (ref. 41)[b]	MoS_2 on rGO[b]	13	250 (dark)	—	Solvothermal, then dip-coat
6	Kibsgaard *et al.* (ref. 35)	MoS_2	0	230	50	Electrodeposition
7	Vrubel and Hu (ref. 36)	Amorphous MoS_3	0	170	—	Electrodeposition
8	Merki *et al.* (2011) (ref. 42)	Amorphous MoS_2	0	200 (14 mA cm^{-2})	40	Electrodeposition
9	Vrubel *et al.* (2012) (ref. 43)	MoS_2 and MoS_3 particles	0	220	50–60	Various, none hydrothermal
10	Huang *et al.* (ref. 44)	Mo_2S_{12}	0	160	39	Drop casting
11	This work	$Co_2Mo_9S_{26}$	0	260	64	Direct hydrothermal

[a] Tafel slopes in mV per decade. [b] Substrate is FTO/reduced graphene oxide (FTO/rGO).

A comparison of Tafel slope data and overpotential requirements to achieve a benchmark current density[37] of 10 mA cm^{-2} for a range of recently-reported metal-chalcogenide HER catalysts on FTO substrates is shown in Table 1. At pH 7, the mixed Co/Mo sulfides prepared on FTO by electrodeposition by Tran *et al.*[23] (Table 1, entry 1) exhibit significantly superior performance to our $Co_2Mo_9S_{26}$-on-FTO materials at the same pH (see above). At pH 0, however, $Co_2Mo_9S_{26}$-on-FTO achieves a current density for the hydrogen evolution reaction of 10 mA cm^{-2} at an overpotential that is essentially the same as that for the aforesaid electrodeposited catalyst at pH 7. Overall, these data suggest that the hydrothermal synthesis method described herein is a viable route for the production of mixed Mo/Co chalcogenides directly on FTO substrates, producing materials that are competent hydrogen evolution electrocatalysts.

To confirm that the current density thus obtained with the $Co_2Mo_9S_{26}$ cathodes was due to the production of hydrogen, gas chromatography was performed on the headspace of sealed cells after extend-time electrolysis (see Experimental section and Fig. S14†). This clearly indicated that hydrogen was the dominant reduction product, with a faradaic yield of 89% (±6%).

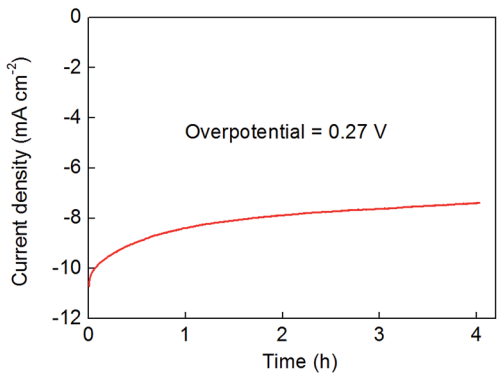

Fig. 6 Controlled potential bulk electrolysis of a 300 nm-thick $Co_2Mo_9S_{26}$ film on an FTO support at a fixed, resistance-corrected overpotential for the hydrogen evolution reaction of 270 mV. The electrolyte was 0.5 M H_2SO_4 and was stirred throughout (see Experimental section for further details).

These extended-time electrolysis experiments also indicated that the activity of the films falls off somewhat over the course of several hours of polarisation at pH 0 (see Fig. 6). In many cases, this drop-off in performance was accompanied by extensive bubble formation on the electrodes which acted to accelerate the cracking and exfoliation of the deposited material. Hence future studies will aim to improve the longevity of these catalysts by tuning film thicknesses (by, for example, adjusting the hydrothermal conditions and reaction times) and also by exploring the effect of additives as a means to deliver superior adhesion of the catalyst to the electrode. Alteration of the transparent conductive metal-oxide substrate may also improve film adhesion and robustness – Fig. S15† shows that when indium-tin oxide (ITO) substrates are used, the decrease in film activity is attenuated somewhat.

Conclusions

In conclusion, we have developed a general synthetic procedure for the direct hydrothermal formation of cobalt-doped molybdenum sulfide on FTO, despite the fact that the FTO substrate is otherwise degraded under hydrothermal conditions in the absence of metal salts. Films of composition $Co_2Mo_9S_{26}$ were formed using this method, and the thicknesses of these films was tuned somewhat by varying the concentrations of the metal salts and thiourea in the hydrothermal deposition solution. These films were found to be good proton reduction electrocatalysts under cathodic bias in 0.5 M H_2SO_4, generating hydrogen at a current density of 10 mA cm^{-2} at 260 mV overpotential and displaying a Tafel slope of 64 mV per decade. Some of the thinner films had substantial translucency, which (combined with their electrochemical performance) renders electrodes produced in this way potential candidates for solar-to-hydrogen applications.

Experimental section

General experimental remarks

$CoSO_4 \cdot 7H_2O$ (99%) and $(NH_4)_6(Mo_7O_{24}) \cdot 4H_2O$ (99%) were purchased from Sigma Aldrich while $SC(NH_2)_2$ (99%) was

supplied by Alfa Aesar. All chemical reagents and solvents were used as purchased. All electrolyte solutions were prepared with reagent grade water (18.2 MΩ cm resistivity), obtained from a Sartorius Arium Comfort combined water system. pH determinations were made with a Hanna HI 9124 waterproof pH meter. UV-Vis spectra were collected in the solid state on a Shimadzu UV-2101PC spectrophotometer. Fluorine-doped tin oxide on glass (FTO) coated plain float electrodes (7 ohms per sheet) were purchased from Hartford Glass Co., Inc. All other materials were obtained as stated in the text. Experiments performed at "room temperature" were carried out at 20 °C.

Synthesis

Preparation of $Co_2Mo_9S_{26}$-on-FTO. FTO substrates were prepared by being soaked for 10 minutes in a KOH/iso-propanol base bath, after which they were rinsed with a 1 M solution of HCl and a copious amount of distilled water. 300 nm-thick films of $Co_2Mo_9S_{26}$-on-FTO were synthesised from a stock solution prepared by mixing together 4.66 mL of an aqueous 50 mM solution of $CoSO_4 \cdot 7H_2O$, 28 mL of an aqueous 7.1 mM solution of $(NH_4)_6Mo_7O_{24} \cdot 4H_2O$, and 70 mL of an aqueous 50 mM solution of $SC(NH_2)_2$ with rigorous stirring (giving a Co : Mo : S ratio of 1 : 6 : 15). Hence this stock solution contained Co, Mo and S in the following overall concentrations: 2.3 mM Co, 13.6 mM Mo and 34.1 mM S. In a typical procedure, 15 mL of this stock solution was poured into a 20 mL Teflon liner, in which a 2.5 × 1 cm^2 FTO substrate was placed with the conductive side facing down at an angle of *ca.* 45° (Fig. S1†). The Teflon liner was then sealed inside a stainless steel reaction vessel and heated at a rate of 1 °C min^{-1} in a convection oven to 180 °C. After 72 hours at this temperature, the vessel was cooled at a rate of 10 °C min^{-1} to room temperature. The vessel was opened in air revealing a colourless solution with pH = *ca.* 8. The product was formed as a grey-black, translucent film on the conductive part of the substrate. The substrate with the film was washed with distilled water and dried in a desiccator over freshly regenerated silica gels at 100 °C. Subsequent annealing of these films at 300 °C under a stream of Ar did not produce any significant improvement in the electrochemical performance of these materials, and so all the results reported herein were obtained without any such annealing.

Thinner films (150 nm-thick) were prepared by the same method, except that the stock solution was prepared by mixing 4.66 mL of an aqueous 20 mM solution of $CoSO_4 \cdot 7H_2O$, 28 mL of an aqueous 2.9 mM solution of $(NH_4)_6Mo_7O_{24} \cdot 4H_2O$, and 70 mL of an aqueous 20 mM solution of $SC(NH_2)_2$ together with rigorous stirring (again giving a Co : Mo : S ratio of 1 : 6 : 15). 15 mL of this stock solution were then poured into a 20 mL Teflon liner containing an FTO substrate and heated as above.

Morphological and compositional characterisation

Raman spectroscopy was carried out on a Horiba Jobin-Yvon LabRam HR800 spectrometer equipped with a 532 nm wavelength laser. To prevent degradation of the sample, a 10% filter and 200 micrometer hole were used. The focus on the surface of the sample was achieved using the controls, with the aid of a microscope with 10× and 50× magnification. Before the measurement the instrument was calibrated using a piece of Si as a standard. Powder X-ray diffraction (PXRD) measurements were performed using a Panalytical XPert-pro diffractometer ($Cu_{K\alpha}$ radiation corresponding to $\lambda = 1.54178$ Å wavelength), operating in a Bragg–Bretano reflection geometry. Scanning electron microscopy was performed in conjunction with an energy-dispersive X-ray (EDX) spectroscopy on a Philips XL30 ESEM with an attached Oxford Instruments x-act EDX detector. All the SEM images and EDX analyses were recorded at an acceleration voltage of 20 kV. Initially, the SEM images were recorded by using the following magnifications: 20×, 100×, 800× and 4000×. The selected areas were then probed by EDX spectroscopy to obtain the elemental composition of the samples. Before running the EDX measurements a Cu foil standard was used for calibrating the measurements. X-ray photoelectron analysis (XPS): as-prepared Co-doped molybdenum sulfide-on-FTO samples were carefully packed and sent to the National EPSRC XPS Users' Service (NEXUS) at Newcastle University, UK. XPS spectra were acquired with a K-Alpha instrument (Thermo Scientific, East Grinstead, UK), using a micro-focused monochromatic AlKα source (X-ray energy 1486.6 eV, spot size 400 × 800 microns). The emission angle was zero degrees and the pass energy was 200 eV for surveys and 40 eV for high resolution. Charge neutralization was enabled. The resulting spectra were referenced to the adventitious C 1s peak (285.0 eV) and were analyzed using the free-to-download CasaXPS software package. Atomic Force Microscopy (AFM) measurements were obtained using a Bruker Dimension Icon AFM. Film steps relative to the FTO substrate were measured over a scan area of 20 μm × 6.7 μm. The step edges for AFM measurements were generated by electrolyzing films for extended time periods in 0.5 M H_2SO_4 according to the general electrochemical methods described below until limited exfoliation of the catalyst material from the FTO substrate had occurred. The relative height of the un-exfoliated catalyst material compared to the bare substrate exposed by exfoliation was then measured. Three different areas were analysed per sample and the data reported are average values for the step sizes that were measured. The thicknesses of the films were measured to ±50 nm thickness. For example, a step measurement on a 300 nm-thick film (taking a 4 μm cut each side of the step) gave a height of 270 nm. The film itself gave an average roughness of 26 nm, whilst for the substrate the roughness was 20 nm Ra.[45] Hence the roughness of the underlying FTO and the roughness of the deposit track reasonably closely. Errors associated with the AFM instrument itself were minimized by using a new tip for each measurement. Atomic absorption spectroscopy (AAS) was performed on a Perkin Elmer Aanalyst400 instrument as follows. To an accurate weight of material (carefully scraped from the FTO substrate) was added 5 mL of aqua regia and the sample was then boiled at 120 °C for 30 minutes, allowed to cool, and transferred to a 25 mL volumetric flask, rinsing all the glassware with deionized water. The samples were diluted to bring them into the linear range to be measured by AAS. A blank sample was also prepared using 5 mL of aqua regia. A series of standards were prepared in the range

0–5 mg L^{-1} for cobalt and 0–50 mg L^{-1} for molybdenum. The standards were prepared in water to match the diluted samples. Cobalt was measured at 240.7 nm using an air acetylene flame. Molybdenum was measured at 313.3 nm using a nitrous oxide/acetylene flame.

Electrochemical methods

General electrochemical methods. Electrochemical studies were performed in a three-electrode configuration (unless otherwise stated) using a CH Instruments CHI760D potentiostat in 0.5 M H_2SO_4, unless otherwise stated. A large surface area carbon felt (Alfa Aesar) was used as the counter electrode (unless otherwise stated), and an Ag/AgCl (NaCl, 3 M) reference electrode (RE 5B, BASi) was used. Working electrodes were washed with deionized water prior to use. Carbon felt counter electrodes were not re-used. Three-electrode potentials were converted to the NHE reference scale using E(NHE) = E(Ag/-AgCl) + 0.209 V. The active area of all working electrodes was on the order of 1 cm^2.

Bulk electrolysis and linear sweep voltammetry. These were performed in a three-electrode configuration (unless otherwise stated) in single compartment electrochemical cells. Solutions were stirred, keeping the same stirring rate for all experiments. Where voltages have been corrected for ohmic resistances, the effective voltage ($V_{effective}$) is given by:[46]

$$V_{effective} = V_{applied} - iR$$

where i is the current flowing through the cell and R is the resistance of the cell. Cell resistances were measured by the *iR* test function available on the CH potentiostats, using the general method developed by He and Faulkner.[47] Briefly, the *iR* test function works by examining the current response to small step changes in voltage relative to a test potential at which no faradaic current flows. In our case, the step change (ΔV) was 0.05 V and the test potential was selected as 0 V *vs.* Ag/AgCl. The *iR* test function on the potentiostat then extrapolates the signal-averaged currents at 54 and 72 ps after the voltage-step edge backwards to obtain a current at $t = 0$, where this current can also be expressed as $\Delta V/R$. R in this case is the solution resistance that is sought. The final parameter that the user must select with this function is the acceptable stability limit of the system at the value of R measured ("% overshoot"): in our case a value of 2% was chosen (default setting on the potentiostat). A Nyquist plot obtained under the same conditions as the *iR* test function is shown in the ESI (Fig. S16†), indicating that the *iR* test function accurately accounts for the R_u component of the total series resistance. Fig. S17† then shows the effect that altering the potential has on the electrochemical impedance of the films. The error associated with the *iR*-correction is dominated by the error associated with gauging the resistance of the solution, where values were found to vary over a range of $R_{measured} \pm 3\%$. Linear sweep voltammograms were recorded at a scan rate of 2 mV s^{-1} unless otherwise stated.

Tafel plots. Tafel plots were obtained in single chamber cells with stirring according to the general methods described above. Plots were generally collected by linear sweep voltammetry at a scan rate of 2 mV s^{-1}, and the reported Tafel slopes are averages of several runs. Where specified, Tafel plots were also constructed by running bulk electrolyses at various potentials. In these cases, the current density was allowed to stabilize for 5 minutes at each potential before being recorded. The overpotentials reported have been corrected for resistive losses.

Gas chromatography

Gas chromatography was conducted in airtight cells according to the general electrochemical procedure given above and using an Agilent Technologies 7890A GC system. During electrolysis, the solution was stirred and the headspace was sampled by gas-tight syringe (volume taken per sampling event = 50 μL) and introduced onto the GC column by direct injection at various intervals. The column used was a 30 metre-long 0.320 mm widebore HP-molesieve column (Agilent). The GC oven temperature was set to 27 °C and the carrier gas was Ar. The front inlet was set to 100 °C. The GC system was calibrated for H_2 using certified standards of hydrogen at a range of volume% in argon supplied by CK Gas Products Limited (UK). Linear fits of volume% *vs.* peak area were obtained, which allowed peak areas to be converted into volume% of H_2 in the cell headspace. Total system headspaces were calculated by filling the cells with water at room temperature. Charges passed were converted into expected volume percentages of hydrogen in the headspace by converting charges to an expected number of moles of gas (by dividing by $2F$ for H_2, where F is the Faraday constant), and then taking the volume of 1 mole of an ideal gas at room temperature and pressure to be 24.5 L. Faradaic efficiencies were then calculated by taking the ratio of gas volume% based on the charge passed to the gas volume% measured by gas chromatography. Faradaic efficiencies were based on the total amount of charge passed, uncorrected for any background or capacitance currents. All gas determinations were performed at least twice, and average faradaic efficiencies are reported in the main text.

Acknowledgements

We acknowledge the University of Glasgow and the EPSRC (grant number EP/K031732/1) for funding. MDS thanks the University of Glasgow for a Kelvin Smith Research Fellowship. We thank Mr Michael Beglan (University of Glasgow) for AAS and UV/vis measurements, Mr Jim Gallagher (University of Glasgow) for assistance with the SEM measurements, the staff at the James Watt Nanofabrication Centre (University of Glasgow) for their assistance with the AFM measurements and Prof. Leroy Cronin and the Glasgow Solar Fuels network (University of Glasgow) for the use of shared facilities. X-ray photoelectron spectra were obtained at the National EPSRC XPS Users' Service (NEXUS) at Newcastle University, an EPSRC Mid-Range Facility. The data which underpin this work are available at http://dx.doi.org/10.5525/gla.researchdata.378 and are licensed CC BY-SA 4.0.

References

1 Y.-Y. Chen, M. Dong, J. Wang and H. Jiao, *J. Phys. Chem. C*, 2012, **116**, 25368.
2 P. M. Mortensen, J.-D. Grunwaldt, P. A. Jensen, K. G. Knudsen and A. D. Jensen, *Appl. Catal., A*, 2011, **407**, 1.
3 J.-F. Paul, S. Cristol and E. Payen, *Catal. Today*, 2008, **130**, 139.
4 M. Pumera, Z. Sofer and A. Ambrosi, *J. Mater. Chem. A*, 2014, **2**, 8981.
5 Y. Min, G. D. Moon, C.-E. Kim, J.-H. Lee, H. Yang, A. Soon and U. Jeong, *J. Mater. Chem. C*, 2014, **2**, 6222.
6 P. Roy and S. K. Srivastava, *J. Mater. Chem. A*, 2015, **3**, 2454.
7 M. A. Bissett, S. D. Worrall, I. A. Kinloch and R. A. W. Dryfe, *Electrochim. Acta*, 2016, **201**, 30.
8 T. Heine, *Acc. Chem. Res.*, 2015, **48**, 65.
9 W. Zhao, R. M. Ribeiro and G. Eda, *Acc. Chem. Res.*, 2015, **48**, 91.
10 X. Xu, W. Yao, D. Xiao and T. F. Heinz, *Nat. Phys.*, 2014, **10**, 343.
11 E. Lhuillier, S. Pedetti, S. Ithurria, B. Nadal, H. Heuclin and B. Dubertret, *Acc. Chem. Res.*, 2015, **48**, 22.
12 T. J. Marks and M. C. Hersam, *Nature*, 2015, **520**, 631.
13 F. H. L. Koppens, T. Mueller, P. Avouris, A. C. Ferrari, M. S. Vitiello and M. Polini, *Nat. Nanotechnol.*, 2014, **9**, 780.
14 M. Buscema, J. O. Island, D. J. Groenendijk, S. I. Blanter, G. A. Steele, H. S. J. van der Zant and A. Castellanos-Gomez, *Chem. Soc. Rev.*, 2015, **44**, 3691.
15 For recent reviews of this topic, see: A. B. Laursen, S. Kegnæs, S. Dahl and I. Chorkendorff, *Energy Environ. Sci.*, 2012, **5**, 5577; Y. Yan, B. Xia, Z. Xu and X. Wang, *ACS Catal.*, 2014, **4**, 1693; J. D. Benck, T. R. Hellstern, J. Kibsgaard, P. Chakthranont and T. F. Jaramillo, *ACS Catal.*, 2014, **4**, 3957; J. Yang and H. S. Shin, *J. Mater. Chem. A*, 2014, **2**, 5979; Q. Lu, Y. Yu, Q. Ma, B. Chen and H. Zhang, *Adv. Mater.*, 2016, **28**, 1917; D. Voiry, J. Yang and M. Chhowalla, *Adv. Mater.*, 2016, **28**, 6197; M. S. Faber and S. Jin, *Energy Environ. Sci.*, 2014, **7**, 3519; M. Zeng and Y. Li, *J. Mater. Chem. A*, 2015, **3**, 14942. See also (for example): J. D. Benck, Z. Chen, L. Y. Kuritzky, A. J. Forman and T. F. Jaramillo, *ACS Catal.*, 2012, **2**, 1916; M. A. Lukowski, A. S. Daniel, F. Meng, A. Forticaux, L. Li and S. Jin, *J. Am. Chem. Soc.*, 2013, **135**, 10274.
16 T. F. Jaramillo, K. P. Jørgensen, J. Bonde, J. H. Nielsen, S. Horch and I. Chorkendorff, *Science*, 2007, **317**, 100.
17 J. K. Nørskov, T. Bligaard, J. Rossmeisl and C. H. Christensen, *Nat. Chem.*, 2009, **1**, 37.
18 J. Bonde, P. G. Moses, T. F. Jaramillo, J. K. Nørskov and I. Chorkendorff, *Faraday Discuss.*, 2008, **140**, 219.
19 J. Zhang, T. Wang, P. Liu, S. Liu, R. Dong, X. Zhuang, M. Chen and X. Feng, *Energy Environ. Sci.*, 2016, **9**, 2789.
20 D. Merki, H. Vrubel, L. Rovelli, S. Fierro and X. Hu, *Chem. Sci.*, 2012, **3**, 2515.
21 J. Staszak-Jirkovský, C. D. Malliakas, P. P. Lopes, N. Danilovic, S. S. Kota, K.-C. Chang, B. Genorio, D. Strmcnik, V. R. Stamenkovic, M. G. Kanatzidis and N. M. Markovic, *Nat. Mater.*, 2016, **15**, 197.
22 H. Zhang, Y. Li, T. Xu, J. Wang, Z. Huo, P. Wan and X. Sun, *J. Mater. Chem. A*, 2015, **3**, 15020.
23 P. D. Tran, S. Y. Chiam, P. P. Boix, Y. Ren, S. S. Pramana, J. Fize, V. Artero and J. Barber, *Energy Environ. Sci.*, 2013, **6**, 2452.
24 H. Zhu, J. Zhang, R. Yanzhang, M. Du, Q. Wang, G. Gao, J. Wu, G. Wu, M. Zhang, B. Liu, J. Yao and X. Zhang, *Adv. Mater.*, 2015, **27**, 4752.
25 J. Xie, H. Zhang, S. Li, R. Wang, X. Sun, M. Zhou, J. Zhou, X. W. Lou and Y. Xie, *Adv. Mater.*, 2013, **25**, 5807.
26 Y. Yan, B. Xia, X. Ge, Z. Liu, J.-Y. Wang and X. Wang, *ACS Appl. Mater. Interfaces*, 2013, **5**, 12794.
27 J. Deng, H. Li, J. Xiao, Y. Tu, D. Deng, H. Yang, H. Tian, J. Li, P. Ren and X. Bao, *Energy Environ. Sci.*, 2015, **8**, 1594.
28 X. Bian, J. Zhu, L. Liao, M. D. Scanlon, P. Ge, C. Ji, H. H. Girault and B. Liu, *Electrochem. Commun.*, 2012, **22**, 128.
29 J. Xie, J. Zhang, S. Li, F. Grote, X. Zhang, H. Zhang, R. Wang, Y. Lei, B. Pan and Y. Xie, *J. Am. Chem. Soc.*, 2013, **135**, 17881.
30 Y.-J. Tang, M.-R. Gao, C.-H. Liu, S.-L. Li, H.-L. Jiang, Y.-Q. Lan, M. Han and S.-H. Yu, *Angew. Chem., Int. Ed.*, 2015, **54**, 12928.
31 Diamond – Crystal and Molecular Structure Visualization, Crystal Impact, H. Putz and K. Brandenburg GbR, Kreuzherrenstr. 102, 53227 Bonn, Germany http://www.crystalimpact.com/diamond, accessed June 2016.
32 E. Payen, S. Kasztelan, S. Houssenbay, R. Szymanski and J. Grimblot, *J. Phys. Chem.*, 1989, **93**, 6501.
33 E. Anastassakis and C. H. Perry, *J. Chem. Phys.*, 1976, **64**, 3604.
34 H. Li, Q. Zhang, C. C. R. Yap, B. K. Tay, T. H. T. Edwin, A. Olivier and D. Baillargeat, *Adv. Funct. Mater.*, 2012, **22**, 1385.
35 J. Kibsgaard, Z. Chen, B. N. Reinecke and T. F. Jaramillo, *Nat. Mater.*, 2012, **11**, 963.
36 H. Vrubel and X. Hu, *ACS Catal.*, 2013, **3**, 2002.
37 C. C. L. McCrory, S. Jung, I. M. Ferrer, S. M. Chatman, J. C. Peters and T. F. Jaramillo, *J. Am. Chem. Soc.*, 2015, **137**, 4347.
38 P. D. Tran, M. Nguyen, S. S. Pramana, A. Bhattacharjee, S. Y. Chiam, J. Fize, M. J. Field, V. Artero, L. H. Wong, J. Loo and J. Barber, *Energy Environ. Sci.*, 2012, **5**, 8912.
39 Y. Sun, C. Liu, D. C. Grauer, J. Yano, J. R. Long, P. Yang and C. J. Chang, *J. Am. Chem. Soc.*, 2013, **135**, 17699.
40 A. B. Laursen, P. C. K. Vesborg and I. Chorkendorff, *Chem. Commun.*, 2013, **49**, 4965.
41 F. Meng, J. Li, S. K. Cushing, M. Zhi and N. Wu, *J. Am. Chem. Soc.*, 2013, **135**, 10286.
42 D. Merki, S. Fierro, H. Vrubel and X. Hu, *Chem. Sci.*, 2011, **2**, 1262.
43 H. Vrubel, D. Merki and X. Hu, *Energy Environ. Sci.*, 2012, **5**, 6136.
44 Z. Huang, W. Luo, L. Ma, M. Yu, X. Ren, M. He, S. Polen, K. Click, B. Garrett, J. Lu, K. Amine, C. Hadad, W. Chen,

A. Asthagiri and Y. Wu, *Angew. Chem., Int. Ed.*, 2015, **54**, 15181.
45 R. K. Leach, Good Practice Guide No. 37: The Measurement of Surface Texture using Stylus Instruments. National Physical Laboratory Publications (UK), http://publications.npl.co.uk/npl_web/pdf/mgpg37.pdf, accessed September, 2016.
46 C. H. Hamann, A. Hamnett and W. Vielstich, *Electrochemistry*, Wiley-VCH, Weinheim, 2007, 2nd edn.
47 P. He and L. R. Faulkner, *Anal. Chem.*, 1986, **58**, 517.